

Noninvasive Immunometabolic Cardiac Inflammation Imaging Using Hyperpolarized Magnetic Resonance

Andrew J.M. Lewis, Jack J. Miller, Angus Z. Lau, Mary K. Curtis, Oliver J. Rider, Robin P. Choudhury, Stefan Neubauer, Charles H. Cunningham, Carolyn A. Carr, Damian J. Tyler

Rationale: Current cardiovascular clinical imaging techniques offer only limited assessment of innate immune cell-driven inflammation, which is a potential therapeutic target in myocardial infarction (MI) and other diseases. Hyperpolarized magnetic resonance (MR) is an emerging imaging technology that generates contrast agents with 10- to 20 000-fold improvements in MR signal, enabling cardiac metabolite mapping.

Objective: To determine whether hyperpolarized MR using $[1-^{13}\text{C}]$ pyruvate can assess the local cardiac inflammatory response after MI.

Methods and Results: We performed hyperpolarized $[1-^{13}\text{C}]$ pyruvate MR studies in small and large animal models of MI and in macrophage-like cell lines and measured the resulting $[1-^{13}\text{C}]$ lactate signals. MI caused intense $[1-^{13}\text{C}]$ lactate signal in healing myocardial segments at both day 3 and 7 after rodent MI, which was normalized at both time points after monocyte/macrophage depletion. A near-identical $[1-^{13}\text{C}]$ lactate signature was also seen at day 7 after experimental MI in pigs. Hyperpolarized $[1-^{13}\text{C}]$ pyruvate MR spectroscopy in macrophage-like cell suspensions demonstrated that macrophage activation and polarization with lipopolysaccharide almost doubled hyperpolarized lactate label flux rates in vitro; blockade of glycolysis with 2-deoxyglucose in activated cells normalized lactate label flux rates and markedly inhibited the production of key proinflammatory cytokines. Systemic administration of 2-deoxyglucose after rodent MI normalized the hyperpolarized $[1-^{13}\text{C}]$ lactate signal in healing myocardial segments at day 3 and also caused dose-dependent improvement in IL (interleukin)-1 β expression in infarct tissue without impairing the production of key reparative cytokines. Cine MRI demonstrated improvements in systolic function in 2-DG (2-deoxyglucose)-treated rats at 3 months.

Conclusions: Hyperpolarized MR using $[1-^{13}\text{C}]$ pyruvate provides a novel method for the assessment of innate immune cell-driven inflammation in the heart after MI, with broad potential applicability across other cardiovascular disease states and suitability for early clinical translation. (*Circ Res.* 2018;122:1084-1093. DOI: 10.1161/CIRCRESAHA.117.312535.)

Key Words: animals ■ cell line ■ magnetic resonance imaging ■ monocytes ■ myocardial infarction

Magnetic resonance (MR) provides exquisite structural imaging of the cardiovascular system, although current proton-based techniques provide only limited assessment of cellular disease processes, including inflammation. Innate immune cells are now understood to be pathophysiological mediators and potential therapeutic targets in myocardial infarction (MI), atherosclerosis, and other cardiovascular diseases.^{1,2} However, clinical translation of a greatly improved understanding of the biology and pathophysiological mechanisms of innate immune cells after MI^{3,4} has been limited, in part, because of the absence of imaging tools to define the monocyte/macrophage response in humans.

Editorial, see p 1039
In This Issue, see p 1033
Meet the First Author, see p 1034

Hyperpolarized MR is an emerging technology in which the magnetic properties of external molecules are manipulated to create molecular MR contrast agents with improvements in signal-to-noise ratio of several orders of magnitude.⁵ One key hyperpolarized substrate, $[1-^{13}\text{C}]$ pyruvate, shows particular promise for cardiovascular applications^{6,7} and enables the detection of its downstream metabolic products, lactate and bicarbonate, at millimolar concentration with spatial localization

Original received December 9, 2017; revision received February 4, 2018; accepted February 12, 2018. In January 2018, the average time from submission to first decision for all original research papers submitted to *Circulation Research* was 13.18 days.

From the Department of Physiology, Anatomy, and Genetics (A.J.M.L., J.J.M., M.K.C., C.A.C., D.J.T.), Department of Physics, Clarendon Laboratory (J.J.M.), Radcliffe Department of Medicine (A.J.M.L., O.J.R., R.P.C., S.N.), and Acute Vascular Imaging Centre (R.P.C.), Radcliffe Department of Medicine, University of Oxford, United Kingdom; and Department of Medical Biophysics, University of Toronto, Ontario, Canada (A.Z.L., C.H.C.).

The online-only Data Supplement is available with this article at <http://circres.ahajournals.org/lookup/suppl/doi:10.1161/CIRCRESAHA.117.312535/-DC1>.

Correspondence to Damian J. Tyler, PhD, Department of Physiology, Anatomy, and Genetics, University of Oxford, Oxford, England OX1 3PT, United Kingdom. E-mail damian.tyler@dpag.ox.ac.uk

© 2018 The Authors. *Circulation Research* is published on behalf of the American Heart Association, Inc., by Wolters Kluwer Health, Inc. This is an open access article under the terms of the [Creative Commons Attribution](https://creativecommons.org/licenses/by/4.0/) License, which permits use, distribution, and reproduction in any medium, provided that the original work is properly cited.

Circulation Research is available at <http://circres.ahajournals.org>

DOI: 10.1161/CIRCRESAHA.117.312535

Novelty and Significance

What Is Known?

- The myocardial inflammatory response that follows myocardial infarction (MI) may be a future clinical therapeutic target.
- There is a lack of clinical imaging tools to assess the cardiac monocyte/macrophage response noninvasively.
- Hyperpolarized magnetic resonance is an emerging imaging technology in which the magnetic resonance imaging signal of key substrates is enhanced by several orders of magnitude, enabling noninvasive cardiac metabolite mapping.

What New Information Does This Article Contribute?

- High hyperpolarized [$1\text{-}^{13}\text{C}$]lactate signal detected from healing infarct tissue in vivo at days 3 and 7 post-MI reflects the monocyte/macrophage inflammatory response.
- High [$1\text{-}^{13}\text{C}$]lactate signal is because of transcriptionally mediated metabolic reprogramming toward glycolysis in activated monocytes/macrophages, which is essential for IL (interleukin)- 1β synthesis.

- Inhibition of monocyte/macrophage metabolic reprogramming with 2-DG (2-deoxyglucose) in vivo reduces cardiac [$1\text{-}^{13}\text{C}$]lactate signal and IL- 1β levels post-MI, providing proof of concept of magnetic resonance-visible immunomodulation.

We here use hyperpolarized magnetic resonance with the [$1\text{-}^{13}\text{C}$]pyruvate tracer in small and large animal models of MI and in cell lines to show that a high [$1\text{-}^{13}\text{C}$]lactate signature provides an imaging biomarker of the monocyte/macrophage response after MI, reflecting metabolic reprogramming in activated monocyte/macrophages, which is intricately linked to their inflammatory function. Our findings identify a new method for imaging the post-MI inflammatory response, which is in principle suitable for rapid clinical translation, and may be of value in a range of other cardiovascular diseases in which innate immune system is implicated.

Nonstandard Abbreviations and Acronyms

18-FDG	^{18}F fluorodeoxyglucose
IL	interleukin
LDH	lactate dehydrogenase
MI	myocardial infarction
MR	magnetic resonance
PDH	pyruvate dehydrogenase
PDK1	pyruvate dehydrogenase kinase 1
PET	positron emission tomography
PFKFB3	6-phosphofructo-2-kinase
PKM	pyruvate kinase
SST2	somatostatin receptor subtype-2
TGF-β	transforming growth factor- β
VEGF-C	vascular endothelial growth factor C

within an organ of interest.⁸ Hyperpolarized [$1\text{-}^{13}\text{C}$]pyruvate has recently been administered to healthy human volunteers in pilot studies with sufficient signal-to-noise ratio to enable cardiac metabolite mapping with high spatial and temporal resolution using multinuclear clinical MRI systems.⁹

Most experimental cardiovascular applications of hyperpolarized MR have to date been conducted with the intention of studying cardiomyocyte metabolism; however, because the monocarboxylate transporters responsible for the cellular uptake of [$1\text{-}^{13}\text{C}$]pyruvate are widely expressed,¹⁰ hyperpolarized substrates could in principle also be used to assess metabolically active, noncardiomyocyte cell populations within hearts, such as innate immune cells. Furthermore, because hyperpolarized [$1\text{-}^{13}\text{C}$]pyruvate MR uniquely assesses ^{13}C label flux through both LDH (lactate dehydrogenase) and PDH (pyruvate dehydrogenase), it holds potential to separate these cell populations by exploiting the intrinsic differences in cellular metabolic machinery and phenotype between immune cells (which are predominantly glycolytic¹¹) and cardiomyocytes (predominantly oxidative¹²). Hyperpolarized MR, therefore, has the potential to overcome the insensitivity of existing cardiac inflammation

imaging techniques and has other potential advantages, including the absence of ionizing radiation, rapid acquisition times, and near-simultaneous, high-resolution, anatomic and functional imaging with accurate metabolite coregistration.

Here, we show that hyperpolarized [$1\text{-}^{13}\text{C}$]pyruvate MR imaging and spectroscopy provide a new approach for imaging the presence and activity of innate immune cells in myocardial tissue by exploiting metabolic reprogramming toward glycolysis in activated monocytes/macrophages, which results in a high [$1\text{-}^{13}\text{C}$]lactate signature. The underlying metabolic reprogramming is essential for monocyte/macrophage inflammatory function, enabling MR-visible pharmacological immunomodulation of the local myocardial inflammatory response to MI.

Methods

The study data are available on reasonable request.

Full details of the experimental methods used, including hyperpolarized MRI, flow cytometry, cell culture, quantitative polymerase chain reaction, and ELISA, are described in the [Online Data Supplement](#).

Statistical Analysis

Data are presented as mean \pm SEM; statistical comparisons are identified in the figures. In brief, where 3 groups were compared, statistical comparisons were by 1-way ANOVA with the Holm-Sidak correction for multiple comparisons, and where 2 experimental groups were compared, statistical comparisons were performed using either paired or unpaired *t* tests as appropriate.

Results

High Hyperpolarized [$1\text{-}^{13}\text{C}$]Lactate Signal at Days 3 and 7 Post-MI Is Because of Monocyte/Macrophage-Driven Inflammation

MI is known to induce an intense local cardiac inflammatory response, including biphasic monocyte/macrophage accumulation.¹³ After an influx of monocytes with a primarily inflammatory phenotype (which peak in number at day 3), the myocardium subsequently recruits monocytes with broadly reparative functions (which are the dominant population by day 7¹³). To determine whether these processes could be assessed using hyperpolarized MRI, we performed either experimental

cryoinfarction or a sham procedure in rats before hyperpolarized MRI, cine MRI, and heart isolation for flow cytometric analysis at day 3 or 7 after surgery (n=6 rats per time point per group). The custom-designed spectral spatial echo-planar imaging sequence provides 3-dimensional cardiac metabolite mapping with a spatial resolution of $2 \times 2 \times 3.8 \text{ mm}^3$ and temporal resolution of 1.8 seconds.¹⁴ [^{13}C]lactate signals were measured from segmentation regions of interest drawn manually around the infarct region (identified as the hypokinetic segments on cine MR) and the spatially average lactate signal normalized by mask size, flip angle, and whole-heart pyruvate signal.

We identified intense [^{13}C]lactate signal in the hypokinetic, healing infarct segments in the separate groups of rats imaged at either day 3 or 7 (Figure 1A and 1B). Quantitative analysis of the lactate signal from infarct regions of interest confirmed a >2-fold increase in [^{13}C]lactate signal when compared with sham-operated controls ($P < 0.01$). In pilot studies, the same high [^{13}C]lactate signature was observed with both coronary artery ligation and cryoinfarction models of MI in rats, although cryoinfarction led to more reproducible infarct sizes and lower mortality and was, therefore, used for the remainder of the study.

Rat hearts were isolated immediately after the MRI assessments for enzymatic digestion and flow cytometric analysis. This confirmed that the high [^{13}C]lactate signature was associated with high numbers of monocytes/macrophages relative to sham-operated controls (Figure 1C). These monocytes/macrophages were as expected predominantly of inflammatory phenotype (CD43^{lo}his48^{hi}) at day 3 and reparative phenotype (CD43^{hi}his48^{lo/int}) at day 7 because CD43 expression in rat monocytes/macrophages exhibits reciprocal expression to the murine Ly6C marker.¹⁵

To mechanistically test the contribution of the monocyte/macrophage population to the [^{13}C]lactate signature, we next performed monocyte/macrophage depletion by administering clodronate liposomes to rats after cryoinfarction (n=6 at each time point). Efficient depletion of the monocyte/macrophage population was confirmed by flow cytometry with a 99% reduction in CD43^{lo}his48^{hi} monocytes/macrophages at day 3 (Figure 1C). Equivalent myocardial injury sizes were confirmed by cine MRI (Online Figure II) with identical increases in end-systolic volume and decreases in ejection fraction seen in both groups relative to sham controls. Monocyte/macrophage depletion with clodronate liposomes essentially normalized the [^{13}C]lactate signal recorded at both time points ($P < 0.05$ at day 3 and $P < 0.01$ at day 7). These findings suggest that monocytes/macrophages are responsible for the [^{13}C]lactate signature detected by hyperpolarized MRI and that hyperpolarized MRI is, therefore, sensitive to the post-MI monocytes/macrophage inflammatory response, although it does not differentiate the 2 phases of the response.

We next asked whether a similar effect would also be present in a more clinically relevant large animal model of MI. To test this, and to provide cross-species validation, we performed hyperpolarized [^{13}C]pyruvate MR imaging at baseline and 7 days after coronary artery balloon-occlusion MI in pigs (n=7). The imaging sequence for these porcine

experiments provides whole-heart coverage with spatial resolution of $10.7 \times 10.7 \text{ mm}^2$ for 6 slices covering the left ventricle from base to apex. The [^{13}C]lactate signal was derived from the apical slices covering the infarct region and normalized to [^{13}C]pyruvate signal intensity.

Again, high [^{13}C]lactate signal was observed in infarct segments at day 7 (Figure 2A), with a 45% increase in [^{13}C]lactate signal when compared with baseline ($P < 0.05$; Figure 2A and 2B). No significant difference in [^{13}C]bicarbonate signal was detected. Histopathologic examination of these pig hearts confirmed that the regions of highest [^{13}C]lactate signal corresponded to high numbers of macrophages (Figure 2C), consistent with the rodent experiments.

Metabolic Reprogramming in Activated Macrophages Causes High Hyperpolarized [^{13}C] Lactate Signal and Is Essential for Proinflammatory Macrophage Function

The hypoxic microenvironment of infarcted myocardium would be expected to provide a significant cellular energetic challenge to infiltrating immune cells, which have a myriad of energetically demanding roles, including proteolysis, phagocytosis, and collagen deposition.^{16,17} Because glycolysis is an oxygen-efficient pathway for ATP synthesis, it follows that high [^{13}C]lactate signal detected in vivo post-MI might reflect metabolic reprogramming in monocytes/macrophages activated by immunologic danger signals released from the necrotic myocardium. To test this, we used an 11.7T vertical bore MR system to measure hyperpolarized [^{13}C]lactate signals spectroscopically from a controlled number of macrophages in suspension. We selected the RAW264.7 macrophage cell line to generate the high numbers of cells required for robust analysis of these data, including kinetic modeling (8×10^7 cells per biological replicate, n=6 biological replicates per group).

We found that polarization of RAW264.7 macrophages using lipopolysaccharide strikingly increased the raw [^{13}C]lactate signal detected spectroscopically from a given number of cells when compared with the same number of saline-treated quiescent cells (Figure 3A). We used kinetic modeling of the dynamic spectroscopic data to estimate pyruvate to lactate exchange constants¹⁸ and multiplied these by the final pyruvate concentration in solution to derive cellular [^{13}C]lactate label flux rates. This analysis confirmed that [^{13}C]lactate label flux rates were approximately doubled in activated macrophages ($P < 0.01$ when compared with saline-treated control cells; Figure 3A), suggesting that both the influx of monocytes/macrophages and also metabolic reprogramming in these activated cells may contribute to the high lactate signature detected after MI in vivo.

Gene expression analysis of RAW264.7 cells using quantitative polymerase chain reaction confirmed that polarization with lipopolysaccharide caused regulation of a panel of genes encoding key glycolytic enzymes, including LDH, PKM (pyruvate kinase), and PFKFB3 (6-phosphofructo-2-kinase/fructose-2,6-bisphosphatase3; Figure 3B), alongside key proinflammatory cytokines, including IL (interleukin)-1 β . These findings suggest that transcriptionally mediated metabolic reprogramming in activated RAW264.7 macrophage-like cells leads to higher glycolytic rates, providing a potential mechanism for the high [^{13}C]lactate signal and flux rates detected.

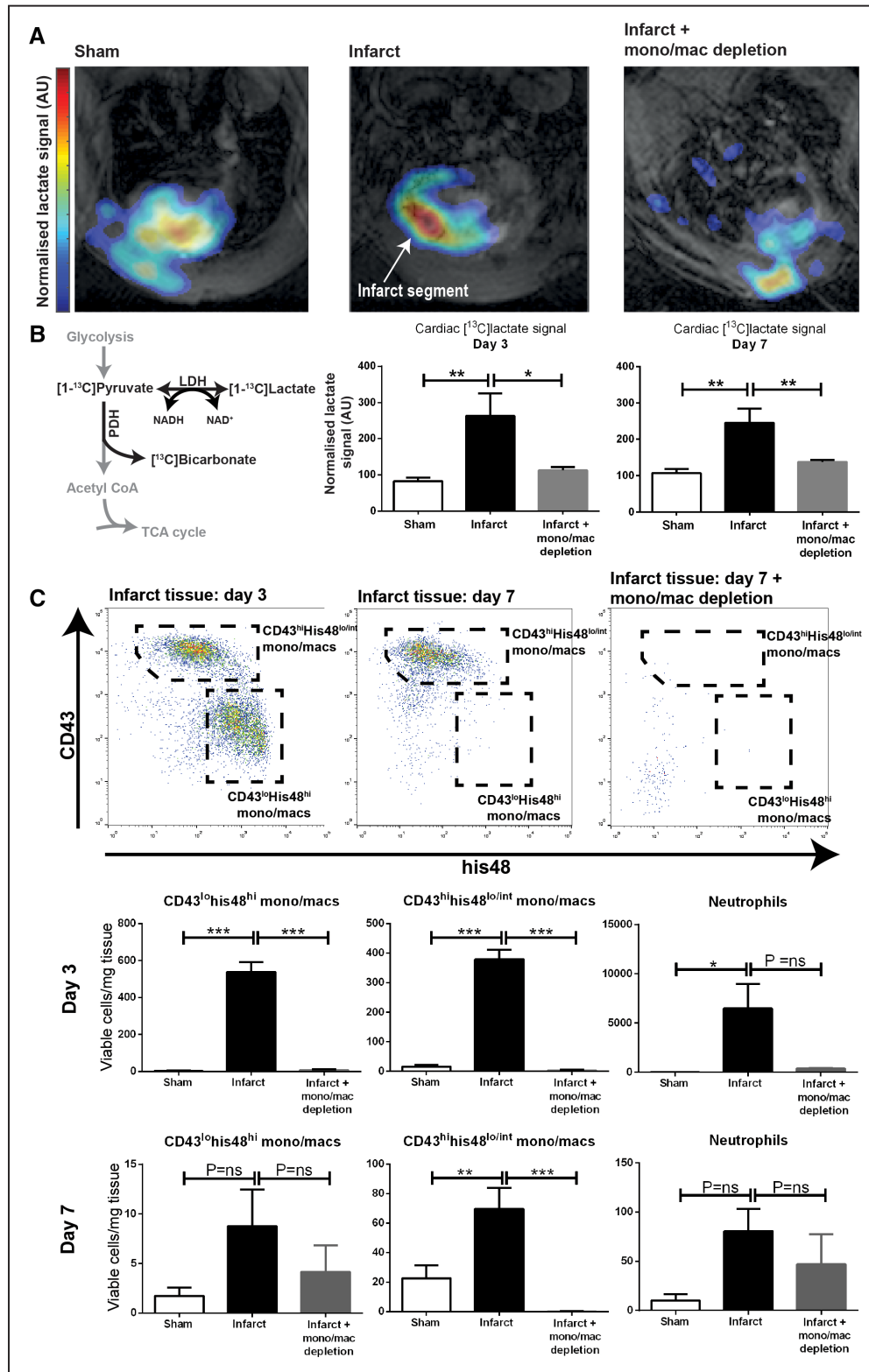


Figure 1. Hyperpolarized lactate generation in a rodent model of cryoinfarction. **A** and **B**, Hyperpolarized MRI demonstrated intense $[1-^{13}\text{C}]$ lactate signal at both days 3 and 7 post-experimental myocardial infarction, which was normalized in rats undergoing pharmacological macrophage depletion ($n=6$ rats assigned per time point per group [$n=36$] to give 4–6 evaluable datasets per time point per group; mean \pm SEM; statistical comparison by 1-way ANOVA with the Holm–Sidak correction for multiple comparisons). Higher lactate signal is detected from the anterior portion of the heart because of some inhomogeneity from the 13C surface coil; lactate signal detected from the chest wall may reflect inflammation in the healing incision. **C**, Flow cytometric analysis of infarct tissue confirmed predominantly inflammatory monocyte/macrophage phenotype ($\text{CD43}^{\text{hi}}\text{his48}^{\text{lo}}$) at day 3 and predominantly reparative ($\text{CD43}^{\text{hi}}\text{his48}^{\text{lo/int}}$) phenotype at day 7 and that both subsets were depleted after the administration of clodronate liposomes. * $P\leq 0.05$, ** $P\leq 0.01$, *** $P\leq 0.001$. LDH indicates lactate dehydrogenase; NADH, nicotinamide adenine dinucleotide; PDH, pyruvate dehydrogenase; and TCA, tricarboxylic acid.

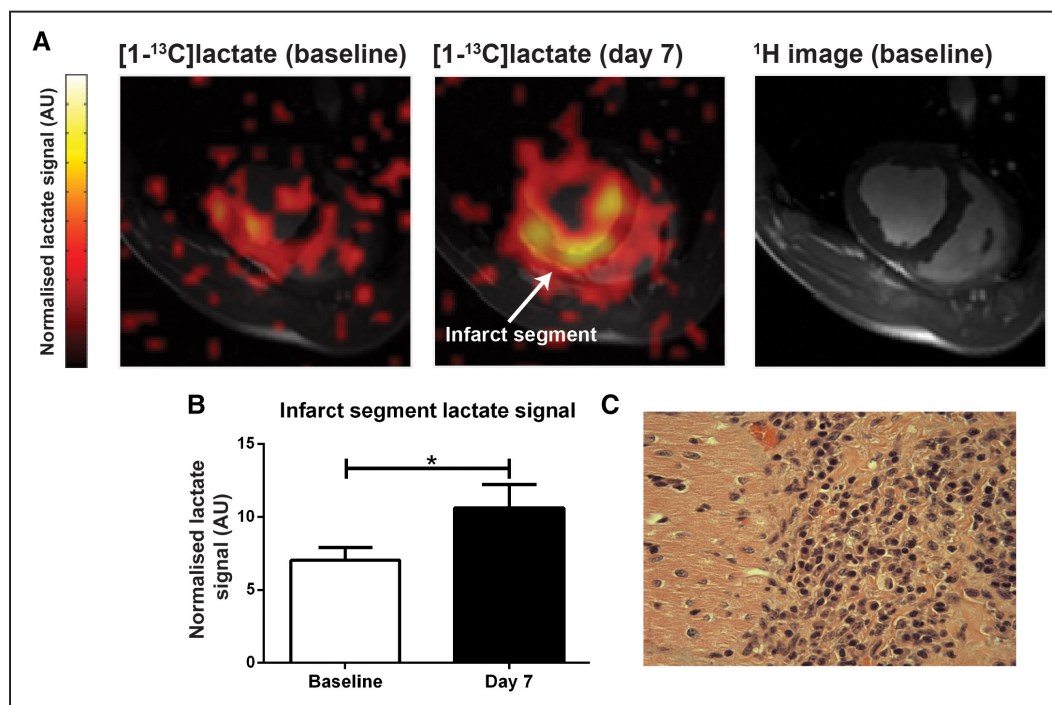


Figure 2. Hyperpolarized lactate generation in a porcine model of myocardial infarction. **A** and **B**, High hyperpolarized lactate signal was again detected in infarct tissue at day 7 in a large animal model of myocardial infarction when compared with the same animal pre-infarction ($n=7$; mean \pm SEM; statistical comparison by paired 2-tailed t test). **C**, The high lactate signal again corresponded to macrophage accumulation on histopathologic examination of the tissue. * $P\leq 0.05$, ** $P\leq 0.01$, *** $P\leq 0.001$.

PDK1 (PDH kinase 1) is a negative regulator of PDH activity and was downregulated, which, therefore, implies an increased PDH flux. This finding suggests that the increase in cellular glycolytic rate is accompanied by an increase in glucose oxidation via PDH, although this was not to a sufficient degree to cause a detectable hyperpolarized [1-¹³C]bicarbonate signal (which reflects PDH flux) in this experiment.

A near-identical pattern of gene regulation was demonstrated in primary murine spleen-derived macrophages, performed to validate these cell line experiments (Online Figure III).

To further understand the relationship between lipopolysaccharide-induced macrophage metabolic reprogramming, hyperpolarized [1-¹³C]lactate signal, and inflammatory cytokine synthesis, we next tested the effect of coinubation of lipopolysaccharide-treated RAW264.7 cells with 2-deoxyglucose, which blocks glycolysis at the level of the hexokinase reaction and stabilizes hypoxia-inducible factor 1 α signaling.¹⁹ We found that 2-DG (2-deoxyglucose) treatment normalized the RAW264.7 macrophage-hyperpolarized [1-¹³C]lactate signal ($P<0.01$) by inhibiting lipopolysaccharide-mediated transcriptional metabolic reprogramming and abrogating the upregulation of LDH, PKM, and PFKFB3 (Figure 3B). 2-DG also strikingly inhibited the synthesis of IL-1 β (which has been reported previously^{19,20}), highlighting a link between hyperpolarized [1-¹³C]lactate signal and cellular inflammatory function in vitro.

MR-Visible Metabolic Immunomodulation Improves Cardiac Systolic Function Post-MI

We next sought to test the links between hyperpolarized [1-¹³C]lactate signal, the macrophage response for MI, and the resulting effects on cardiac remodeling and systolic function in vivo,

with the aim of understanding whether hyperpolarized MR may have a potential future role as an imaging biomarker to test immunomodulation after MI. Although nonselective immunosuppression in this setting is known to be associated with impaired cardiac wound healing and a risk of ventricular rupture,^{21,22} selective targeting of the phase 1 monocyte/macrophage pro-inflammatory response pathways may be a viable strategy to improve cardiac remodeling and systolic function.^{23,24}

To address this, we administered either 2-DG or saline to rats between days 0 and 3 after cryoinfarction ($n=12$). We found that 2-DG caused dose-dependent downregulation of IL-1 β gene expression in infarct tissue (Figure 4A) with a 66% reduction at the higher dose of 1g/kg per day in 2 divided doses ($P<0.01$). This dose of 2-DG also reduced the high hyperpolarized [1-¹³C]lactate signal detected by hyperpolarized MR at day 3 ($P<0.05$), which was suppressed to a level similar to that observed in sham-treated animals in previous experiments. Because our previous cell depletion experiments have suggested that elevated cardiac [1-¹³C]lactate signal post-MI is caused by monocytes/macrophages, this finding implies sufficient delivery of 2-DG to the cardiac monocyte/macrophage population to reproduce the anti-inflammatory effect demonstrated in vitro. It furthermore highlights a mechanistic link between hyperpolarized [1-¹³C]lactate signal and cardiac tissue-level inflammation.

The 2-DG dosing strategy (0–72 hours) was selected with the intent of suppressing primarily the phase 1 inflammatory response while preserving tissue repair processes in phase 2 (maximal at day 7). To determine whether this was the case, we measured the day 7 expression of cytokines and growth factors with roles in cardiac repair, revascularization, and mature collagen deposition,²⁵ including TGF- β (transforming

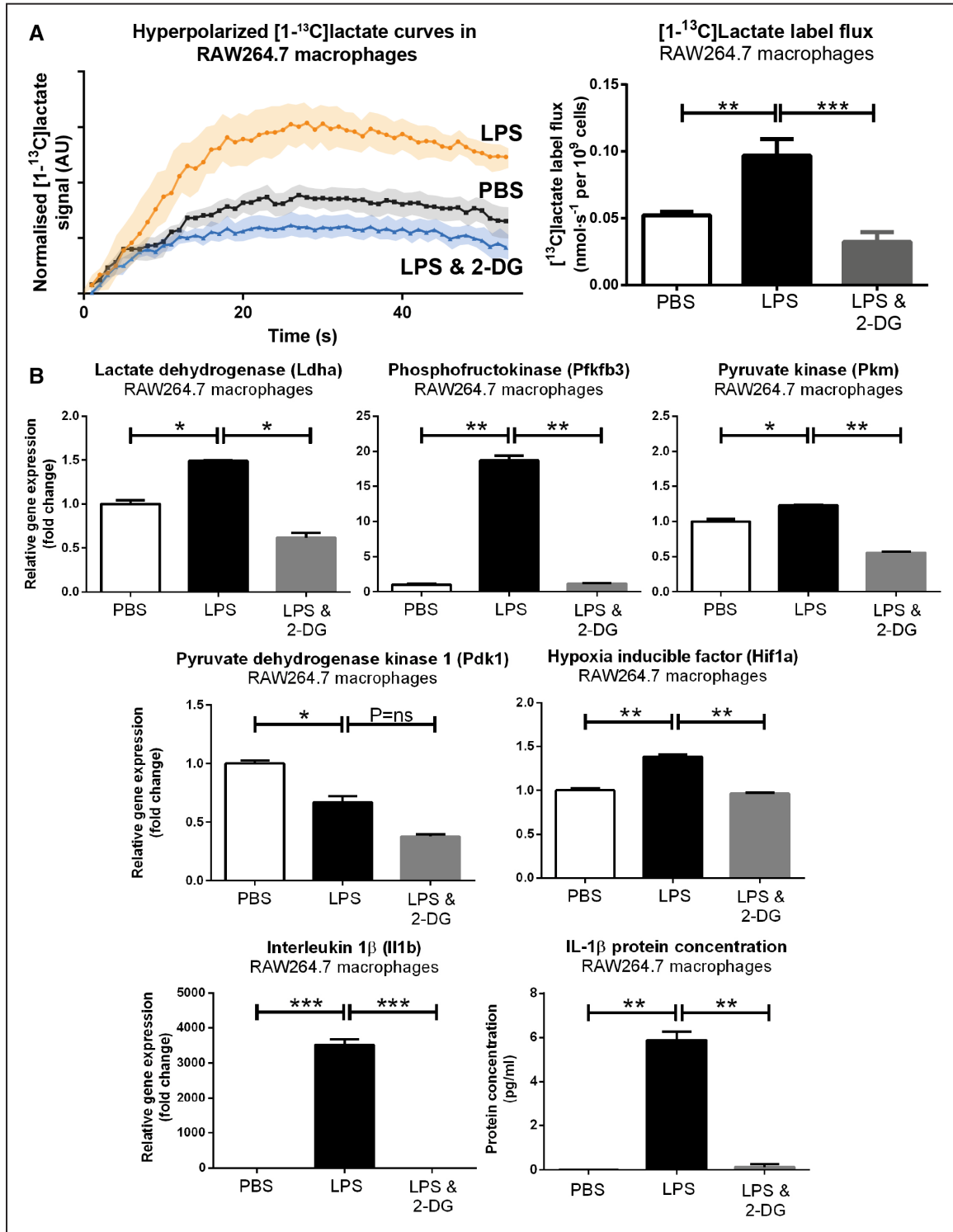


Figure 3. Hyperpolarized lactate generation in activated RAW264.7 cell suspensions. **A**, Hyperpolarized MR experiments in RAW264.7 cell suspensions demonstrated high lactate signal and label flux rates in activated cells, which was normalized by 2-DG (2-deoxyglucose; 80×10^6 cells per biological replicate; mean \pm SEM; $n=5-6$ evaluable datasets per group; 1-way ANOVA with the Holm-Sidak correction for multiple comparisons; PBS; lipopolysaccharide [LPS]). $[^{13}\text{C}]$ lactate signal intensity curves (normalized to $[1-^{13}\text{C}]$ pyruvate signal) after $[1-^{13}\text{C}]$ pyruvate injection are presented; shaded region denotes SEM. $[^{13}\text{C}]$ lactate label flux rates were derived by kinetic modeling of the spectroscopic data multiplied by the final pyruvate concentration in solution. **B**, LPS caused regulation of a panel of genes encoding glycolytic enzymes and proinflammatory cytokines, which were attenuated after administration of 2-DG. Similar patterns of gene regulation were demonstrated in primary murine spleen-derived macrophages (Online Figure II). * $P \leq 0.05$, ** $P \leq 0.01$, *** $P \leq 0.001$. IL indicates interleukin.

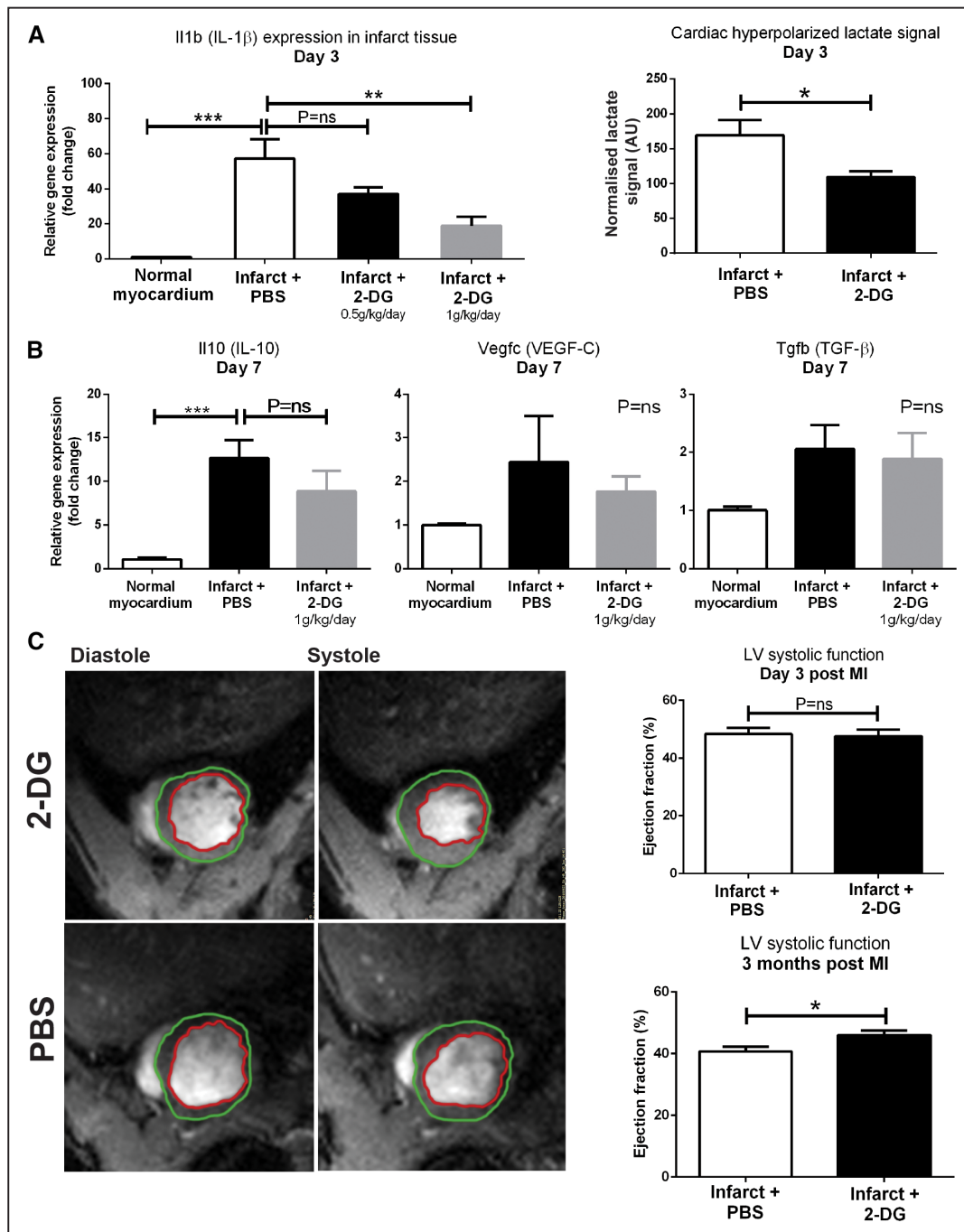


Figure 4. Systemic administration of 2-DG (2-deoxyglucose) to rats post-myocardial infarction (MI) caused dose-dependent downregulation of IL (interleukin)-1 β gene expression in infarct tissue and also normalized hyperpolarized [^{13}C]lactate signal ($n=4-5$ evaluable datasets per group). 2-DG had no significant effect on expression of genes encoding the proreparative factors IL-10, VEGF-C (vascular endothelial growth factor C), and TGF- β (transforming growth factor- β ; $n=3-4$ biological replicates per group; 1-way ANOVA with the Holm-Sidak correction for multiple comparisons). Cine MRI analysis demonstrated that 2-DG attenuated the rate of decline in left ventricle (LV) systolic function between day 3 and 3 months ($n=9$ biological replicates per group to give 7–9 evaluable data sets; unpaired unequal variance t test). * $P\leq 0.05$, ** $P\leq 0.01$, *** $P\leq 0.001$.

growth factor- β), IL-10, and VEGF-C (vascular endothelial growth factor C; Figure 4B) in healthy control rats and rats undergoing cryoinfarction with either saline treatment or 2-DG treatment between days 0 and 3 ($n=12$). We found no significant difference in the expression of these factors. These findings suggest that this regimen of 2-DG selectively modulates phase 1 of the immune response post-MI. Consistent with this,

no incidence of ventricular rupture was detected by cine MRI in any 2-DG-treated rat.

Because selective modulation of the phase 1 inflammatory response is a potential therapeutic target after MI, we next asked what effect MR-visible immunomodulation of IL-1 β synthesis with 2-DG would have on cardiac remodeling and systolic function, assessed using cine MRI. Control- and

2-DG–treated rats had equivalent ventricular volumes and systolic function at day 3, which suggests equivalent acute injury size (Online Figure IV). The left ventricles in both groups dilated by around 30% between day 3 and 3 months during remodeling, and the rate of increase of end-systolic volume was modestly attenuated in 2-DG–treated rats, with a 5% absolute improvement in ejection fraction at 3 months ($P < 0.05$; Figure 4C). These findings suggest that 2-DG–mediated immunomodulation post-MI can be monitored noninvasively using hyperpolarized MRI and may improve cardiac remodeling by selectively targeting the phase I inflammatory response.

Discussion

Acute MI remains a leading cause of heart failure, despite effective reperfusion strategies.²⁶ The development of new imaging technologies to define pathways, which could be targeted in the days after MI with the aim of improving cardiac remodeling and reducing heart failure, therefore, represents an important and clinically relevant goal.

Our finding that the influx and metabolic reprogramming of activated innate immune cells within infarct tissue can be assessed using hyperpolarized [1-¹³C]pyruvate MR provides an approach by which MR could be used to better understand innate immune cell biology in human cardiovascular disease. Conventional proton MR-based techniques, including T_1 parametric mapping and T_2 weighted imaging, are known to be insensitive to immune cell number after MI because any signal change attributable to these cells is masked by much larger changes in ^1H T_1 and T_2 resulting from edema and collagen deposition.^{27,28} It follows that the combination of hyperpolarized [1-¹³C]pyruvate MR (to assess inflammation via [¹³C]lactate mapping) with ^1H T_1 , T_2 , and gadolinium-based contrast agent techniques, including extracellular volume mapping (for tissue characterization and functional imaging) could be used to provide a more comprehensive assessment of the interplay between the myocardial inflammatory response and the resulting tissue architecture and ventricular function than is possible currently. Furthermore, because the immunologic danger signals released from necrotic myocardium polarize quiescent innate immune cells via their conserved pattern recognition/toll-like receptors,^{29,30} inflammation imaging with hyperpolarized [1-¹³C]pyruvate MR may well be broadly applicable across other cardiovascular disease states involving innate immune cell activation, including atherosclerosis, myocarditis, and endocarditis.

Previous studies using positron emission tomography (PET) of the 18-fluorodeoxyglucose (¹⁸FDG) tracer have demonstrated high cardiac ¹⁸FDG uptake in the days after MI, which may reflect similar cellular processes to those resulting in high [1-¹³C]lactate signal in this study.³¹ However, cardiac ¹⁸FDG PET can be confounded by high background glucose uptake by the myocardium, and its ability to detect the smaller signal resulting from immune cell activity is, therefore, critically dependent on artificial suppression of cardiac carbohydrate metabolism using, for example, high fat/low carbohydrate diets in clinical studies, and the mode of anesthesia used in preclinical studies.³¹ The failure rate of cardiac carbohydrate uptake suppression in humans is reported to be 20% to 30%.³²

Newer PET tracers targeting macrophage cell surface proteins (such as ⁶⁸Ga-DOTATATE or ⁶⁸Ga-DOTA-TOC, which

bind SST₂ [somatostatin receptor subtype-2], and ⁶⁸Ga-citrate, which binds lactoferrin) show promise for the identification of inflammatory activity of monocytes and macrophages.³³ Furthermore, because SST₂ is exclusively expressed in pro-inflammatory M1-type macrophages, ⁶⁸Ga-DOTATATE offers reliable imaging of inflammatory activity in active atherosclerotic plaques,^{33,34} avoiding the limitation of ¹⁸FDG myocardial spillover for coronary imaging. These tracers have been clinically translated to human use and in a clinical investigation, ⁶⁸Ga-DOTA-TOC demonstrated consistent uptake in patients with myocarditis or subacute MI,³⁵ as well as in a patient with cardiac involvement from sarcoidosis.³⁶ Balanced against these studies, in a detailed preclinical investigation, neither ⁶⁸Ga-DOTATATE nor ⁶⁸Ga-citrate showed appreciable uptake in myocardial infarct tissue after MI.³⁷ Further leukocyte tracers, including those targeting the chemokine receptor CXCR4 (C-X-C chemokine receptor type 4)³⁸ or translocator protein,³⁹ are in development although they remain to be tested post-MI. In future clinical studies, the performance of these PET tracers for post-MI inflammation imaging could be prospectively tested alongside alternative MRI technologies, including 19F MRI using emulsified perfluorocarbons,^{40,41} which shows promise in preclinical models or iron oxide nanoparticles, as well as hyperpolarized [1-¹³C]pyruvate.

Hyperpolarized [1-¹³C]pyruvate offers several advantages over ¹⁸FDG for cardiac applications. First, the ability to image the downstream products of glucose metabolism offers the potential to improve specificity when compared to measurement of glucose uptake because of the divergent metabolic phenotypes of glycolytic immune cells and oxidative cardiomyocytes. Furthermore, hyperpolarized MR enables imaging without the need for artificial suppression of cardiomyocyte metabolism, the absence of ionizing radiation (enabling longitudinal studies in humans), faster acquisition times (cardiac hyperpolarized MR acquisitions typically last 2–5 minutes compared with cardiac gated PET acquisitions, which can take >30 minutes), and the ability to normalize the [1-¹³C]lactate signal to tissue delivery rates of the [1-¹³C]pyruvate substrate, which may be particularly important after MI when tissue delivery rates of the tracer may be impaired by either an epicardial coronary stenosis or microvascular dysfunction. Furthermore, because lactate is increasingly recognized to be an immunologic danger signal in its own right,²⁰ assessment of the lactate pool size might provide a more fundamental assessment of innate immune cell immunometabolic function after MI than glucose uptake alone. It is, however, not yet clear whether clinical cardiac hyperpolarized MRI will achieve or exceed the spatial resolution of PET (which is typically 4–6 mm for ¹⁸FDG⁴²) because clinical 13C MR coils and sequences are still in their infancy. Furthermore, clinical grade hyperpolarizers are currently only available in a few centers worldwide, unlike PET cyclotrons and scanners.

IL-1 β is a cytokine known to control processes determining myocardial remodeling post-MI,^{23,43,44} and most therapeutic studies to date have focussed on downstream targeting of the cytokine using monoclonal antibodies. Although this approach avoids the potentially deleterious effects of nonselective immunosuppression with, for example, corticosteroids,

the lack of routine availability of human myocardial tissue for cytokine assay or assessment of inflammation post-MI limits the potential for individualization of therapy or validation of dosing strategy.⁴⁵ Given that the degree of myocardial injury and subsequent inflammation after acute coronary syndromes is highly heterogeneous, it is perhaps not surprising that clinical trials involving largely unselected patients with MI have had variable results to date.^{46–48} Hyperpolarized MR may, therefore, have an early role in the identification of patient subgroups with the highest degree of myocardial inflammation, who might be expected to derive the most benefit from currently available immunomodulatory therapies, such as anakinra or canakinumab. In the future, hyperpolarized MR may also have utility in the development of drugs targeting upstream pathways responsible for proinflammatory cytokines by immune cells. Although 2-deoxyglucose experiences unpredictable pharmacokinetics and toxicity and is unlikely to be tested in humans with MI,⁴⁹ newer immunometabolic modulators are in advancing stages of development and may provide new classes of drugs for immunomodulation.⁵⁰

In summary, hyperpolarized MR using [1-¹³C]pyruvate provides a novel noninvasive assessment of cardiac innate immune cell-driven inflammation by detecting [1-¹³C]lactate signal resulting from induction of an immunometabolic signaling axis, which is essential for inflammatory cytokine production and controls cardiac remodeling. In addition to potential future applications in human ischemic heart disease, this technique may have broad value in other forms of inflammatory disease with important advantages over existing techniques.

Sources of Funding

This research was supported by the British Heart Foundation Centre of Research Excellence (Oxford), the National Institute for Health Research Oxford Biomedical Research Centre Programme, the British Heart Foundation Fellowship (FS/10/002/28078 and FS/14/17/30634), the British Heart Foundation Programme Grant (RG/11/9/28921), and the Engineering and Physical Sciences Research Council Doctoral Training Centre and Prize Fellowship (EP/M508111/1) grants. R.P. Choudhury was supported by the British Heart Foundation Centre of Research Excellence (Oxford), the British Heart Foundation Oxford Centre for Regenerative Medicine, and the Tripartite Immunometabolism Consortium–Novo Nordisk Foundation (grant No. NNF15CC0018486).

Disclosures

None.

Acknowledgments

A.J.M. Lewis conceived the experiment, conducted experimental work, analyzed data, and drafted the manuscript. J.J. Miller designed MR imaging sequence and methodology for data analysis and performed rodent hyperpolarized MRI experiments. A.Z. Lau designed MR imaging sequence and methodology for data analysis and performed porcine hyperpolarized MRI and infarction experiments. M.K. Curtis performed experimental work. C.A. Carr, O.J. Rider, R.P. Choudhury, S. Neubauer, and D.J. Tyler were responsible for resources and supervised the preclinical experiments. All authors reviewed and commented on the manuscript.

References

- Swirski FK, Nahrendorf M. Leukocyte behavior in atherosclerosis, myocardial infarction, and heart failure. *Science*. 2013;339:161–166. doi: 10.1126/science.1230719.
- Frangogiannis NG. The inflammatory response in myocardial injury, repair, and remodeling. *Nat Rev Cardiol*. 2014;11:255–265. doi: 10.1038/nrcardio.2014.28.
- Swirski FK, Nahrendorf M, Etzrodt M, Wildgruber M, Cortez-Retamozo V, Panizzi P, Figueiredo JL, Kohler RH, Chudnovskiy A, Waterman P, Aikawa E, Mempel TR, Libby P, Weissleder R, Pittet MJ. Identification of splenic reservoir monocytes and their deployment to inflammatory sites. *Science*. 2009;325:612–616. doi: 10.1126/science.1175202.
- Dutta P, Courties G, Wei Y, et al. Myocardial infarction accelerates atherosclerosis. *Nature*. 2012;487:325–329. doi: 10.1038/nature11260.
- Ardenkjaer-Larsen JH, Fridlund B, Gram A, Hansson G, Hansson L, Lerche MH, Servin R, Thaning M, Golman K. Increase in signal-to-noise ratio of > 10,000 times in liquid-state NMR. *Proc Natl Acad Sci USA*. 2003;100:10158–10163.
- Day SE, Kettunen MI, Gallagher FA, Hu DE, Lerche M, Wolber J, Golman K, Ardenkjaer-Larsen JH, Brindle KM. Detecting tumor response to treatment using hyperpolarized ¹³C magnetic resonance imaging and spectroscopy. *Nat Med*. 2007;13:1382–1387. doi: 10.1038/nm1650.
- Schroeder MA, Cochlin LE, Heather LC, Clarke K, Radda GK, Tyler DJ. In vivo assessment of pyruvate dehydrogenase flux in the heart using hyperpolarized carbon-13 magnetic resonance. *Proc Natl Acad Sci USA*. 2008;105:12051–12056.
- Schroeder MA, Clarke K, Neubauer S, Tyler DJ. Hyperpolarized magnetic resonance: a novel technique for the in vivo assessment of cardiovascular disease. *Circulation*. 2011;124:1580–1594. doi: 10.1161/CIRCULATIONAHA.111.024919.
- Cunningham CH, Lau JY, Chen AP, Geraghty BJ, Perks WJ, Roifman I, Wright GA, Connelly KA. Hyperpolarized ¹³C metabolic MRI of the human heart: initial experience. *Circ Res*. 2016;119:1177–1182. doi: 10.1161/CIRCRESAHA.116.309769.
- Enerson BE, Drewes LR. Molecular features, regulation, and function of monocarboxylate transporters: implications for drug delivery. *J Pharm Sci*. 2003;92:1531–1544. doi: 10.1002/jps.10389.
- Kelly B, O'Neill LA. Metabolic reprogramming in macrophages and dendritic cells in innate immunity. *Cell Res*. 2015;25:771–784. doi: 10.1038/cr.2015.68.
- Neubauer S. The failing heart—an engine out of fuel. *N Engl J Med*. 2007;356:1140–1151. doi: 10.1056/NEJMra063052.
- Nahrendorf M, Swirski FK, Aikawa E, Stangenberg L, Wurdinger T, Figueiredo JL, Libby P, Weissleder R, Pittet MJ. The healing myocardium sequentially mobilizes two monocyte subsets with divergent and complementary functions. *J Exp Med*. 2007;204:3037–3047. doi: 10.1084/jem.20070885.
- Miller JJ, Lau AZ, Teh I, Schneider JE, Kinches P, Smart S, Ball V, Sibson NR, Tyler DJ. Robust and high resolution hyperpolarized metabolic imaging of the rat heart at 7 T with 3D spectral-spatial EPI. *Magn Reson Med*. 2016;75:1515–1524. doi: 10.1002/mrm.25730.
- Barnett-Vanes A, Sharrock A, Birrell MA, Rankin S. A single 9-colour flow cytometric method to characterise major leukocyte populations in the rat: validation in a model of LPS-induced pulmonary inflammation. *PLoS One*. 2016;11:e0142520. doi: 10.1371/journal.pone.0142520.
- Nahrendorf M, Swirski FK. Monocyte and macrophage heterogeneity in the heart. *Circ Res*. 2013;112:1624–1633. doi: 10.1161/CIRCRESAHA.113.300890.
- Frangogiannis NG. The immune system and cardiac repair. *Pharmacol Res*. 2008;58:88–111. doi: 10.1016/j.phrs.2008.06.007.
- Zierhut ML, Yen YF, Chen AP, Bok R, Albers MJ, Zhang V, Tropp J, Park I, Vigneron DB, Kurhanewicz J, Hurd RE, Nelson SJ. Kinetic modeling of hyperpolarized ¹³C1-pyruvate metabolism in normal rats and TRAMP mice. *J Magn Reson*. 2010;202:85–92. doi: 10.1016/j.jmr.2009.10.003.
- Tannahill GM, Curtis AM, Adamik J, et al. Succinate is an inflammatory signal that induces IL-1 β through HIF-1 α . *Nature*. 2013;496:238–242. doi: 10.1038/nature11986.
- Yang L, Xie M, Yang M, Yu Y, Zhu S, Hou W, Kang R, Lotze MT, Billiar TR, Wang H, Cao L, Tang D. PKM2 regulates the Warburg effect and promotes HMGB1 release in sepsis. *Nat Commun*. 2014;5:4436.
- Roberts R, DeMello V, Sobel BE. Deleterious effects of methylprednisolone in patients with myocardial infarction. *Circulation*. 1976;53:1204–1206.
- Bulkley BH, Roberts WC. Steroid therapy during acute myocardial infarction. A cause of delayed healing and of ventricular aneurysm. *Am J Med*. 1974;56:244–250.
- Leuschner F, Dutta P, Gorbato R, et al. Therapeutic siRNA silencing in inflammatory monocytes in mice. *Nat Biotechnol*. 2011;29:1005–1010. doi: 10.1038/nbt.1989.
- Ruparelina N, Chai JT, Fisher EA, Choudhury RP. Inflammatory processes in cardiovascular disease: a route to targeted therapies. *Nat Rev Cardiol*. 2017;14:133–144. doi: 10.1038/nrcardio.2016.185.

25. Frangogiannis NG, Mendoza LH, Lewallen M, Michael LH, Smith CW, Entman ML. Induction and suppression of interferon-inducible protein 10 in reperfused myocardial infarcts may regulate angiogenesis. *FASEB J*. 2001;15:1428–1430.
26. Gerber Y, Weston SA, Enriquez-Sarano M, Manemann SM, Chamberlain AM, Jiang R, Roger VL. Atherosclerotic burden and heart failure after myocardial infarction. *JAMA Cardiol*. 2016;1:156–162. doi: 10.1001/jamacardio.2016.0074.
27. Fernández-Jiménez R, García-Prieto J, Sánchez-González J, Agüero J, López-Martín GJ, Galán-Arriola C, Molina-Iracheta A, Doohan R, Fuster V, Ibáñez B. Pathophysiology underlying the bimodal edema phenomenon after myocardial ischemia/reperfusion. *J Am Coll Cardiol*. 2015;66:816–828. doi: 10.1016/j.jacc.2015.06.023.
28. Fernández-Jiménez R, Sánchez-González J, Agüero J, et al. Myocardial edema after ischemia/reperfusion is not stable and follows a bimodal pattern: imaging and histological tissue characterization. *J Am Coll Cardiol*. 2015;65:315–323. doi: 10.1016/j.jacc.2014.11.004.
29. Shishido T, Nozaki N, Yamaguchi S, Shibata Y, Nitobe J, Miyamoto T, Takahashi H, Arimoto T, Maeda K, Yamakawa M, Takeuchi O, Akira S, Takeishi Y, Kubota I. Toll-like receptor-2 modulates ventricular remodeling after myocardial infarction. *Circulation*. 2003;108:2905–2910. doi: 10.1161/01.CIR.0000101921.93016.1C.
30. Oyama J, Blais C Jr, Liu X, Pu M, Kobzik L, Kelly RA, Bourcier T. Reduced myocardial ischemia-reperfusion injury in toll-like receptor 4-deficient mice. *Circulation*. 2004;109:784–789. doi: 10.1161/01.CIR.0000112575.66565.84.
31. Lee WW, Marinelli B, van der Laan AM, et al. PET/MRI of inflammation in myocardial infarction. *J Am Coll Cardiol*. 2012;59:153–163. doi: 10.1016/j.jacc.2011.08.066.
32. Dweck MR, Aikawa E, Newby DE, Tarkin JM, Rudd JH, Narula J, Fayad ZA. Noninvasive molecular imaging of disease activity in atherosclerosis. *Circ Res*. 2016;119:330–340. doi: 10.1161/CIRCRESAHA.116.307971.
33. Li X, Bauer W, Kreissl MC, Weirather J, Bauer E, Israel I, Richter D, Riehl G, Buck A, Samnick S. Specific somatostatin receptor II expression in arterial plaque: (68)Ga-DOTATATE autoradiographic, immunohistochemical and flow cytometric studies in apoE-deficient mice. *Atherosclerosis*. 2013;230:33–39. doi: 10.1016/j.atherosclerosis.2013.06.018.
34. Tarkin JM, Joshi FR, Evans NR, et al. Detection of Atherosclerotic Inflammation by 68Ga-DOTATATE PET Compared to [18F]FDG PET Imaging. *J Am Coll Cardiol*. 2017;69:1774–1791. doi: 10.1016/j.jacc.2017.01.060.
35. Lapa C, Reiter T, Li X, Werner RA, Samnick S, Jahns R, Buck AK, Ertl G, Bauer WR. Imaging of myocardial inflammation with somatostatin receptor based PET/CT - A comparison to cardiac MRI. *Int J Cardiol*. 2015;194:44–49. doi: 10.1016/j.ijcard.2015.05.073.
36. Reiter T, Werner RA, Bauer WR, Lapa C. Detection of cardiac sarcoidosis by macrophage-directed somatostatin receptor 2-based positron emission tomography/computed tomography. *Eur Heart J*. 2015;36:2404. doi: 10.1093/eurheartj/ehv278.
37. Thackeray JT, Bankstahl JP, Wang Y, Korf-Klingebiel M, Walte A, Wittneben A, Wollert KC, Bengel FM. Targeting post-infarct inflammation by PET imaging: comparison of (68)Ga-citrate and (68)Ga-DOTATATE with (18)F-FDG in a mouse model. *Eur J Nucl Med Mol Imaging*. 2015;42:317–327. doi: 10.1007/s00259-014-2884-6.
38. Thackeray JT, Derlin T, Haghighi A, Napp LC, Wang Y, Ross TL, Schäfer A, Tillmanns J, Wester HJ, Wollert KC, Bauersachs J, Bengel FM. Molecular imaging of the chemokine receptor CXCR4 after acute myocardial infarction. *JACC Cardiovasc Imaging*. 2015;8:1417–1426. doi: 10.1016/j.jcmg.2015.09.008.
39. Hupe HC, Thackeray J, Postema J, Wang Y, Ross TL, Wollert K, Bankstahl J, Bengel F. Myocardial infarction is associated with neuroinflammation—a systemic analysis using TSPO-targeted molecular imaging. *J Nucl Med*. 2016;57:404–404.
40. Temme S, Jacoby C, Ding Z, Bönner F, Borg N, Schrader J, Flögel U. Technical advance: monitoring the trafficking of neutrophil granulocytes and monocytes during the course of tissue inflammation by noninvasive 19F MRI. *J Leukoc Biol*. 2014;95:689–697. doi: 10.1189/jlb.0113032.
41. Ye YX, Basse-Lüsebrink TC, Arias-Loza PA, Kocoski V, Kampf T, Gan Q, Bauer E, Sparka S, Helluy X, Hu K, Hiller KH, Boivin-Jahns V, Jakob PM, Jahns R, Bauer WR. Monitoring of monocyte recruitment in reperfused myocardial infarction with intramyocardial hemorrhage and microvascular obstruction by combined fluorine 19 and proton cardiac magnetic resonance imaging. *Circulation*. 2013;128:1878–1888. doi: 10.1161/CIRCULATIONAHA.113.000731.
42. Rosenbaum D, Millon A, Fayad ZA. Molecular imaging in atherosclerosis: FDG PET. *Curr Atheroscler Rep*. 2012;14:429–437. doi: 10.1007/s11883-012-0264-x.
43. Dewald O, Zymek P, Winkelmann K, Koerting A, Ren G, Abou-Khamis T, Michael LH, Rollins BJ, Entman ML, Frangogiannis NG. CCL2/Monocyte Chemoattractant Protein-1 regulates inflammatory responses critical to healing myocardial infarcts. *Circ Res*. 2005;96:881–889. doi: 10.1161/01.RES.0000163017.13772.3a.
44. Sager HB, Heidt T, Hulsmans M, Dutta P, Courties G, Sebas M, Wojtkiewicz GR, Tricot B, Iwamoto Y, Sun Y, Weissleder R, Libby P, Swirski FK, Nahrendorf M. Targeting interleukin-1 β reduces leukocyte production after acute myocardial infarction. *Circulation*. 2015;132:1880–1890. doi: 10.1161/CIRCULATIONAHA.115.016160.
45. Matthews PM, Rabiner I, Gunn R. Non-invasive imaging in experimental medicine for drug development. *Curr Opin Pharmacol*. 2011;11:501–507. doi: 10.1016/j.coph.2011.04.009.
46. Ridker PM, Thuren T, Zalewski A, Libby P. Interleukin-1 β inhibition and the prevention of recurrent cardiovascular events: rationale and design of the Canakinumab Anti-inflammatory Thrombosis Outcomes Study (CANTOS). *Am Heart J*. 2011;162:597–605. doi: 10.1016/j.ahj.2011.06.012.
47. O'Donoghue ML, Glaser R, Cavender MA, et al; LATITUDE-TIMI 60 Investigators. Effect of losmapimod on cardiovascular outcomes in patients hospitalized with acute myocardial infarction: a randomized clinical trial. *JAMA*. 2016;315:1591–1599. doi: 10.1001/jama.2016.3609.
48. Newby LK, Marber MS, Melloni C, et al; SOLSTICE Investigators. Losmapimod, a novel p38 mitogen-activated protein kinase inhibitor, in non-ST-segment elevation myocardial infarction: a randomised phase 2 trial. *Lancet*. 2014;384:1187–1195. doi: 10.1016/S0140-6736(14)60417-7.
49. Maschek G, Savaraj N, Priebe W, Braunschweiger P, Hamilton K, Tidmarsh GF, De Young LR, Lampidis TJ. 2-deoxy-D-glucose increases the efficacy of adriamycin and paclitaxel in human osteosarcoma and non-small cell lung cancers in vivo. *Cancer Res*. 2004;64:31–34.
50. O'Neill LA, Kishton RJ, Rathmell J. A guide to immunometabolism for immunologists. *Nat Rev Immunol*. 2016;16:553–565. doi: 10.1038/nri.2016.70.

Circulation Research

JOURNAL OF THE AMERICAN HEART ASSOCIATION



Noninvasive Immunometabolic Cardiac Inflammation Imaging Using Hyperpolarized Magnetic Resonance

Andrew J.M. Lewis, Jack J. Miller, Angus Z. Lau, Mary K. Curtis, Oliver J. Rider, Robin P. Choudhury, Stefan Neubauer, Charles H. Cunningham, Carolyn A. Carr and Damian J. Tyler

Circ Res. 2018;122:1084-1093; originally published online February 12, 2018;
doi: 10.1161/CIRCRESAHA.117.312535

Circulation Research is published by the American Heart Association, 7272 Greenville Avenue, Dallas, TX 75231
Copyright © 2018 American Heart Association, Inc. All rights reserved.
Print ISSN: 0009-7330. Online ISSN: 1524-4571

The online version of this article, along with updated information and services, is located on the
World Wide Web at:

<http://circres.ahajournals.org/content/122/8/1084>

Free via Open Access

Data Supplement (unedited) at:

<http://circres.ahajournals.org/content/suppl/2018/02/12/CIRCRESAHA.117.312535.DC1>

Permissions: Requests for permissions to reproduce figures, tables, or portions of articles originally published in *Circulation Research* can be obtained via RightsLink, a service of the Copyright Clearance Center, not the Editorial Office. Once the online version of the published article for which permission is being requested is located, click Request Permissions in the middle column of the Web page under Services. Further information about this process is available in the [Permissions and Rights Question and Answer](#) document.

Reprints: Information about reprints can be found online at:
<http://www.lww.com/reprints>

Subscriptions: Information about subscribing to *Circulation Research* is online at:
<http://circres.ahajournals.org/subscriptions/>

Supplemental Material

The authors declare that the study data are available upon reasonable request.

Rodent experiments

Animal models

All experiments were performed in accordance with relevant legislation with personal, project and institutional licenses granted under the UK Animals (Scientific Procedures) Act 1986 for rodent experiments and under a protocol approved by the institutional animal care and use committee at the University of Toronto for pig experiments.

Rodent MI models

Female Wistar rats aged 7-10 weeks weighing 200-250 g were supplied by Envigo UK. Standard chow and bedding was provided. Female rats were selected on account of reported better survival following infarct surgery. Anaesthesia was induced using inhaled 4% isoflurane in medical oxygen in all rats, reduced to 2% isoflurane in medical oxygen for maintenance of anaesthesia. The trachea was intubated and the lungs ventilated, and a left thoracotomy performed. In pilot experiments, a polyethylene tube was sutured across the left anterior descending coronary artery for 40 minutes and removed. In subsequent experiments using the cryoinjury method, the heart was exteriorised and a 9mm aluminium cryoprobe cooled to the temperature of liquid nitrogen applied to the antero-apical myocardium for 15 seconds. The chest was closed in layers and analgesia provided with meloxicam and buprenorphine.

Rodent hyperpolarized MRI

Anaesthesia was induced and maintained using inhaled isoflurane at the same doses as was used for infarction surgery (4% isoflurane in medical oxygen for induction and 2% for maintenance). All experiments were conducted with rats in the fed state between 0600 and 1300 using a homeothermic imaging cradle. Approximately 40 mg [1-¹³C]pyruvic acid, doped with 15 mM OX063 trityl radical and trace Dotarem gadolinium chelate, was hyperpolarized and dissolved in a prototype hyperpolarizer as described previously¹. 2 mL of the resulting 80 mM pyruvate solution with liquid state polarization of 30 – 40 % was injected manually over 20 s via a preplaced tail vein catheter.

Hyperpolarized magnetic resonance imaging was performed using a Varian 7 T DDR system, with an actively detuned transmit/surface receive setup consisting of a 72 mm dual-tuned ¹H/¹³C proton/carbon birdcage volume coil with a 40 mm two-channel ¹³C surface receive array with an integrated preamp (Rapid Biomedical GMBH, Rimpf, Germany).

Multicoil images were recombined according to the method of McKenzie² with coil sensitivity maps inferred from the acquired data, prior to reconstruction as described previously³. Magnitude images were temporally integrated with respect to time, and an estimate of the corresponding baseline noise subtracted (without Rician noise correction owing to fact that integrated images had a minimal imaginary component and SNR >>2⁴). Segmentation regions-of-interest (ROIs) were then manually drawn around the infarct region, as identified via corresponding FLASH CINE MR, and the

spatially averaged lactate signal corrected for by mask size, flip angle, and whole heart pyruvate.

ECG gated cardiac cine images were acquired to include long axis cines and a contiguous series of short axis cines covering the left ventricle from base to apex. Prospectively gated proton cardiac images were obtained with a volume transmit / four-channel surface receive array together with a rodent FLASH Cine sequence with no acceleration and a simple sum-of-squares multi-coil reconstruction as previously documented (TR 4.6 ms, TE 1.66 ms, 128x128 matrix, 51.2 x 51.2 mm FOV; 1.6 mm slice thickness; nominal in-plane resolution 400 μ m; 4 averages; 28 cardiac frames; scan time ~10 minutes per animal). Volumetric analysis was performed using cmr42 software (Circle Cardiovascular Imaging, Calgary, Canada) by an experienced analyst blinded to experimental group.

Flow cytometry

Following perfusion with 50 ml cold Hanks' balanced salt solution (HBSS) to remove circulating immune cells, hearts were isolated and the infarcted region was excised from the heart, including the border zone. The infarct segments were triturated using surgical scissors. Fine tissue fragments underwent digestion to single cell suspension in a collagenase II solution (500 units/ml in Hanks' balanced salt solution) for 30 minutes at 37 °C with intermittent agitation. 1×10^6 cells were incubated with 1 μ l mouse anti-rat CD32 to minimise non-specific binding of Fc expressing cells. Cells were stained with 1 μ l Zombie Violet™ Live/Dead for 20 minutes at 4 °C, prior to further staining with the antibody cocktail. F

Flow cytometric experiments were performed at the flow cytometry core facility at the Sir William Dunn School of Pathology, University of Oxford. For cytometric experiments, cell suspensions were analysed using either a Beckman Coulter CyAn™ flow cytometer or a MoFlo® Astrios™ cell sorter. Compensation was adjusted manually using single colour controls or in accordance with the principle of fluorescence minus one (FMO) where necessary. Gating strategies (which for rat experiments were adapted from a strategy devised by Barnett-Vanes *et al*⁶) are presented in online Fig I.

Porcine experiments

Myocardial infarction

All animal experiments were carried out under a protocol approved by the institutional animal care and use committee at the University of Toronto. Female Yorkshire pigs ($n = 7$, weight 25–30 kg) were used in this study. Myocardial ischemia was induced for 60 minutes using a previously described percutaneous left anterior descending artery (LAD) occlusion model with 60 minutes of ischaemia^{6, 7}. Imaging experiments were performed at baseline prior to LAD occlusion and 7 days following the infarct.

Porcine hyperpolarized MR imaging

Hyperpolarized magnetic resonance was performed using a 3 T GE MR750 scanner (GE Healthcare, Waukesha, WI) equipped with the multinuclear spectroscopy (MNS) hardware package. A ¹³C transmit volume coil and a dual-tuned ¹H/¹³C receive-only surface coil (Rapid MR International, Columbus, Ohio) were used for the animal experiments as previously described⁸. The positioning over the heart was confirmed

by 3-plane ^1H scout images acquired using the ^1H -tuned surface coil, that provided visualization of the fiduciary markers placed on the coil. For anatomical landmarking, cardiac-gated breath-held SSFP CINE images were acquired in the short axis view (pulse repetition times (TR) = 4.2 ms, echo time = 1.8 ms, field of view-24 cm, slice thickness 5-mm, spacing 5-mm, matrix size = 224×224).

Infarct assessment was performed using a T_1 -weighted inversion recovery gradient-echo sequence in the short axis view (TR = 6.3 ms, echo time = 3 ms, field of view 24 cm, flip 15 = angle°, matrix size = 224×192 , 2 RR intervals, inversion time (300–350 ms) adjusted to null normal myocardial signal). Delayed enhancement images were acquired 12 min following intravenous injection of 8–12 mL of gadolinium–DTPA (0.2 mmol/kg; Magnevist, Bayer Healthcare, Wayne, NJ).

[1- ^{13}C]pyruvic acid (15 mL, concentration 83 mM, pH 7.4) was hyperpolarized in a HyperSense DNP polarizer (Oxford Instruments, Abingdon, UK) as described previously. A time-resolved, cardiac and respiratory gated ^{13}C spiral sequence was used⁹ to image [1- ^{13}C]pyruvate, lactate, and bicarbonate in the porcine heart. In brief, the cardiac and respiratory gated acquisition acquires six slices during each 2.5 s repetition time (TR) ordered from base to apex. In-plane spatial encoding was performed using a single-shot spiral trajectory, with the readout length modified depending on the number of slices used (8192×1 points, field of view 48 cm, $T_{\text{read}} = 32$ ms (10.7×10.7 mm² in-plane resolution) for six slices, time per slice 60 ms). The imaging sequence provides spatial resolution of 10.7×10.7 mm² for six slices covering the left ventricle from base to apex. Hyperpolarized [1- ^{13}C] myocardial lactate was quantified by summing the lactate signal from slices covering the infarct segments normalised to the corresponding average [1- ^{13}C]pyruvate signal intensity.

Histology

7 days after a 60 min LAD occlusion, the heart was removed and fixed in 10% neutral buffered Formalin, whole-mount histology sections were made with 5 mm bread loaf slices, imbedded in paraffin and then cut at thickness at 5µm. These were then mounted to glass slides, processed with standard H&E staining. The images were acquired using a Leica DM-LB2 microscope equipped with DFC480 camera (Leica Microsystems, Wetzlar, Germany), on the slides of anterior wall of left ventricle, at 3-3.5cm above apex.

Cultured macrophage experiments

Cell culture

RAW264.7 cells were supplied by ATCC and maintained in RPMI-1640 medium supplemented with 10% foetal bovine serum at 37 °C and 5% CO₂ using either 75ml or 175ml tissue culture flasks (Corning). Cells were passaged when they reached >70% confluency and used between passage number 10-20.

To create primary spleen derived macrophages, mouse spleens were passed through a 70 micron mesh and red blood cells lysed by incubation for 2 minutes in a hypotonic lysis solution (Insight Biotechnology). The resulting splenocytes were washed and plated at $4\text{--}6 \times 10^6$ cells per well of a 6 well plate. Culture medium was RPMI-1640 medium supplemented with 10% FBS, 5 ng/ml M-CSF and 1% penicillin/streptomycin. Non-adherent cells were removed and the medium changed every other day. Experiments were performed upon cells at day 6.

Lipopolysaccharides derived from *Escherichia Coli* were supplied by Sigma and were used at 1 µg/ml. 2-DG was also supplied by Sigma and was used at a final concentration of 1mM following pilot dose ranging experiments which demonstrated effective suppression of lactate production and minimal cytotoxicity.

Hyperpolarized MR in cell suspensions

Pyruvic acid (5 µl) was mixed with gadolinium (0.5 µl of 1:50 Dotarem) and OX063 radical and hyperpolarized using a Hypersense polarizer for 30 minutes. RAW264.7 cells were detached from culture flask using Accutase® cell detachment solution (Biolegend) and washed prior to a semi-automated cell count and resuspension at 8×10^7 cells in 1 ml medium at 37°C. The cell suspension was added to an NMR tube and placed in an 11.7 T magnet with warm air blown across the tube to maintain a temperature of approximately 37 °C. Hyperpolarized [1-¹³C]pyruvate solution was then produced by dissolution using 4.5 ml Tris/NaOH buffer and 1 ml of the resulting solution mixed with the cell suspension by injection through a polyethylene tube. The time between cell resuspension and dissolution was approximately 5 minutes. ¹³C NMR signals were acquired over 1 minute.

Dynamic [¹³C]lactate signals were fitted to the kinetic model of Zierhut¹⁰ to derive label exchange rate constants ($k_{\text{pyr-lac}}$) and multiplied by the final pyruvate concentration in solution to estimate [1-¹³C]lactate label flux rates.

qPCR

Approximately 30mg heart tissue was homogenised in RLT lysis buffer (Qiagen) and RNA extracted using RNeasy mini columns (Qiagen). The integrity of the extracted RNA was confirmed by NanoDrop spectrophotometry (Thermo Scientific); all samples had A₂₆₀:A₂₈₀ ratio of >2. RNA was reverse transcribed using a high-capacity cDNA reverse transcription kit (Thermo Scientific).

TaqMan® primers were used in 20ul qPCR reactions which were run in duplicate using a StepOnePlus qPCR system (Thermo Scientific). Gene expression was normalised to expression of murine 18s pre-ribosomal RNA (RAW264.7 or primary spleen derived macrophage studies) or 45s pre-ribosomal RNA (Rn03928990_g1, rat tissues) and expressed according to the $2^{-\Delta\Delta\text{CT}}$ method. Details of the gene expression assays used are provided below in Online Table I:

Online Table I: List of gene expression assays used.

Gene symbol	Gene name	TaqMan® assay identity
Pkm	Pyruvate kinase	Mm00834102_gH
Ldha	Lactate dehydrogenase	Mm01612132_g1
Pdk1	Pyruvate dehydrogenase kinase 1	Mm00554300_m1
Pfkfb3	6-phosphofructo-2-kinase	Mm00504650_m1
IL1b	Interleukin 1β	Mm00434228_m1
hif1A	Hypoxia inducible factor 1	Mm00468869_m1
Rn18S	Pre-ribosomal RNA	Mm03928990_g1
Il10	Interleukin 10	Rn01483988_g1
Tgfb	Transforming growth factor beta	Rn01475965_g1
Vegfc	Vascular endothelial growth factor C	Rn01488076_m1
Rn18S	45S pre-ribosomal RNA	Rn03928990_g1

Enzyme linked immunosorbent assay (ELISA)

Cells were harvested from 6-well plates using a cell scraper and resuspended in 1ml phosphate buffered saline prior to homogenisation using spin columns (Qiashredder, Qiagen). Enzyme linked immunosorbent assays were performed upon the resultant cell homogenates using assay kits according the manufacturers' instructions. The IL-1β kit was supplied by eBioscience

Excluded animals and methodological and reporting aspects

All animals were eligible to enter the study if they survived infarct or sham procedure. A formal randomisation process was not performed,

though experimental group and treatment allocation was concealed to investigators prior to MRI data analysis using code identifiers held by a separate investigator and not released until after analysis. There were no adequate prior estimates of [¹³C]lactate effect size/variability to inform a prospective power calculation due to novelty and the planned n = 36 in the initial study was based on feasibility.

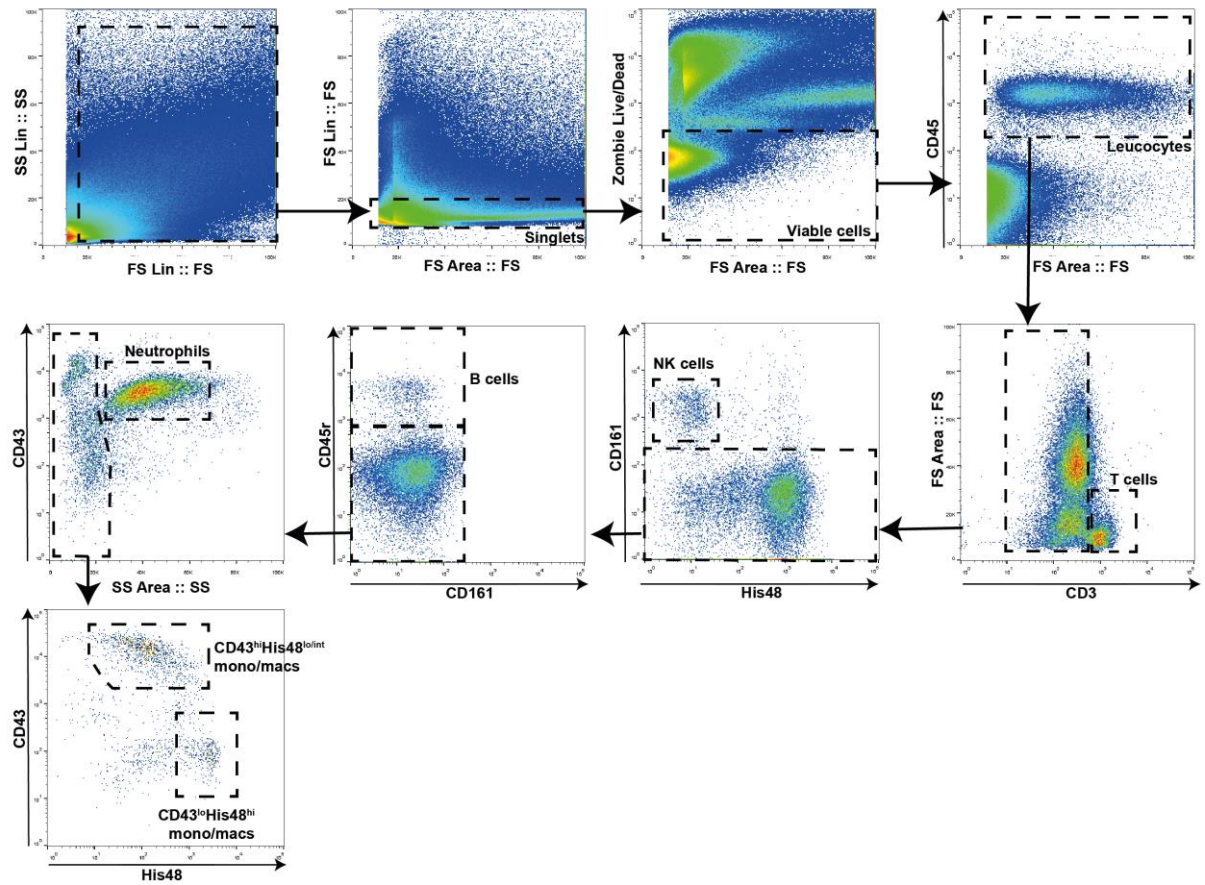
Figure 1: N = 6 rats per group assigned (n = 36 total initially survived surgery and entered the study). N = 2 rats died post operatively (day 3 infarct x1, day 7 infarct x1), n = 3 datasets could not be analysed due to very low hyperpolarized MRI signal-to-noise ratio and were excluded (day 3 sham x1, day 7 infarct x1, day 7 clodronate x1) to give 31 evaluable hyperpolarized MR datasets.

Figure 2: N = 7 pigs, all datasets evaluable.

Figure 3: No animals used or excluded.

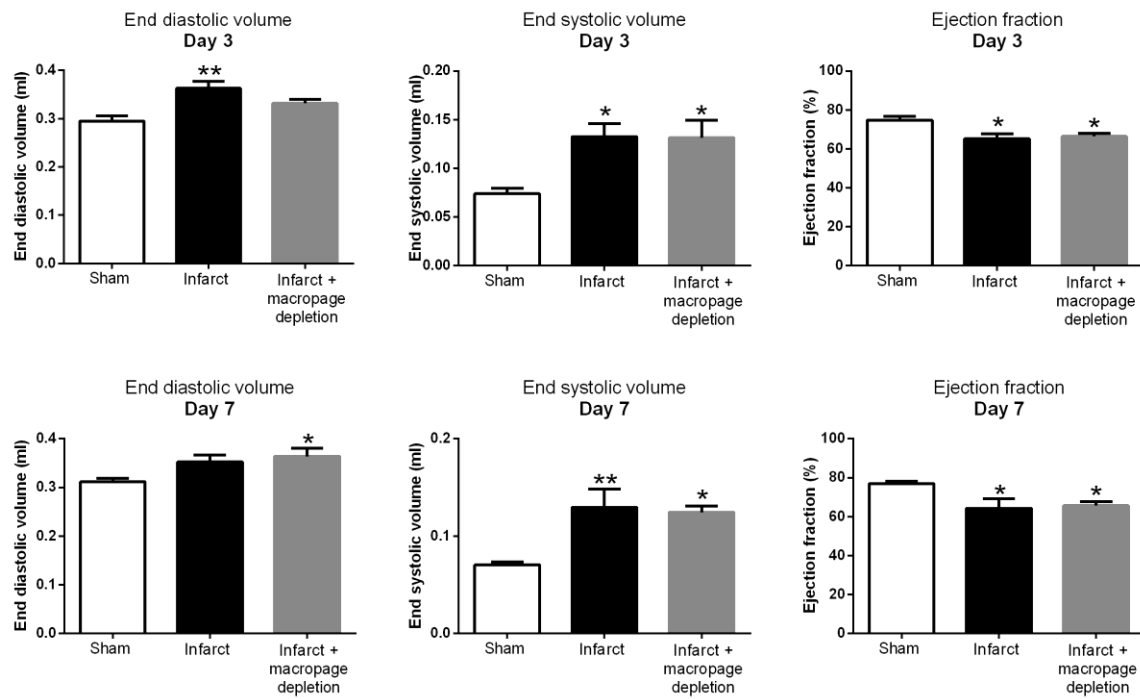
Figure 4: Panel a, gene expression analysis, n = 12, no exclusions. Hyperpolarized MR, n = 10 assigned, n = 1 dataset from saline group excluded from hyperpolarized MRI analysis due to very low signal-to-noise ratio. Panel b, n = 12 assigned, n = 1 excluded from control infarct group as died following surgery. Panel C, n = 18 assigned, 1 rat in the PBS group died and 1 dataset at 3 months (also PBS group) was not evaluable due to poor ECG triggering.

Online Figure I



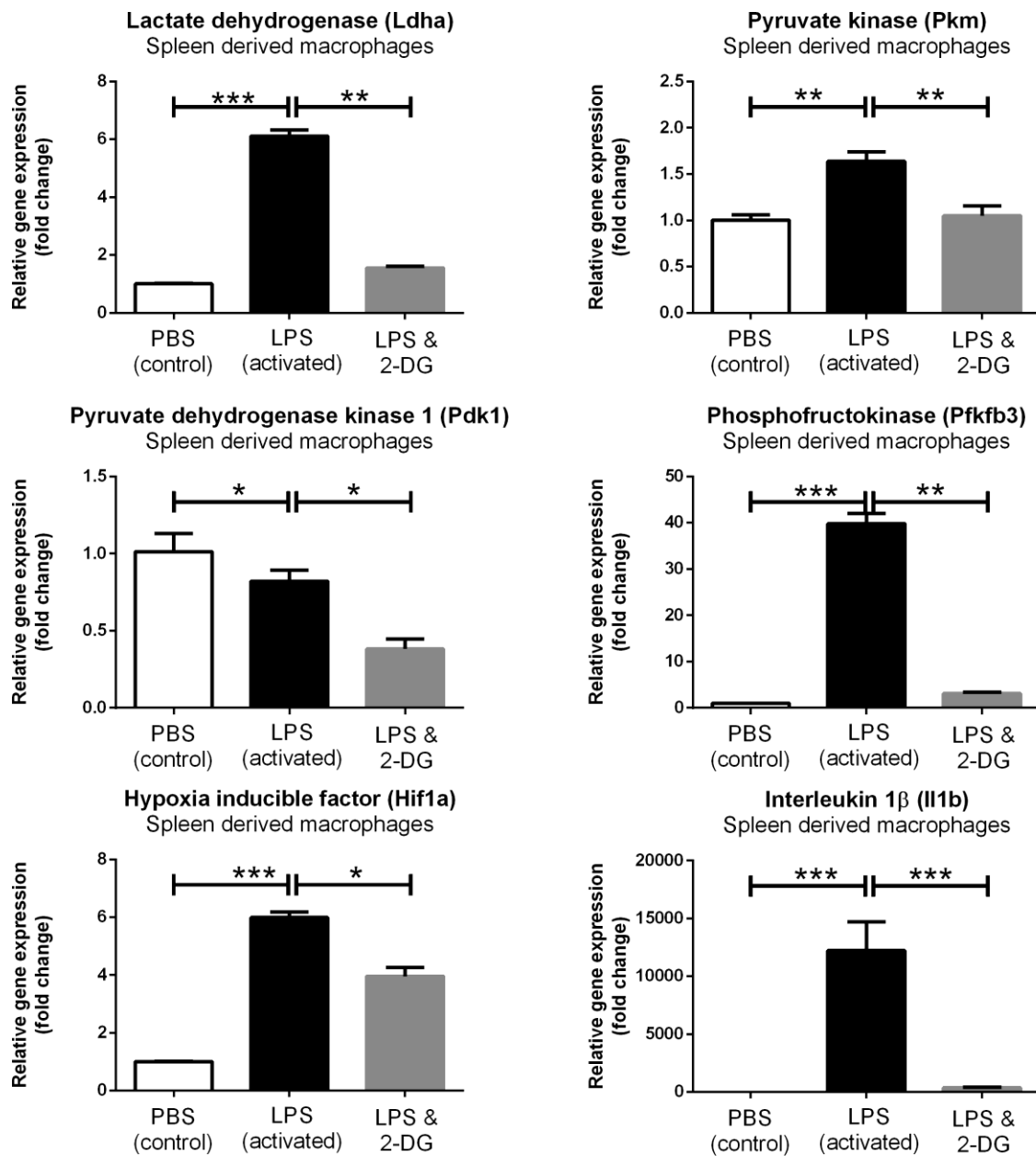
Online Figure I: The flow cytometric gating strategy was adapted from a method described by Barnett-Vanes *et al*⁵. After gating out debris and doublets, viable cells were selected and the leucocyte population identified and categorised.

Online Figure II



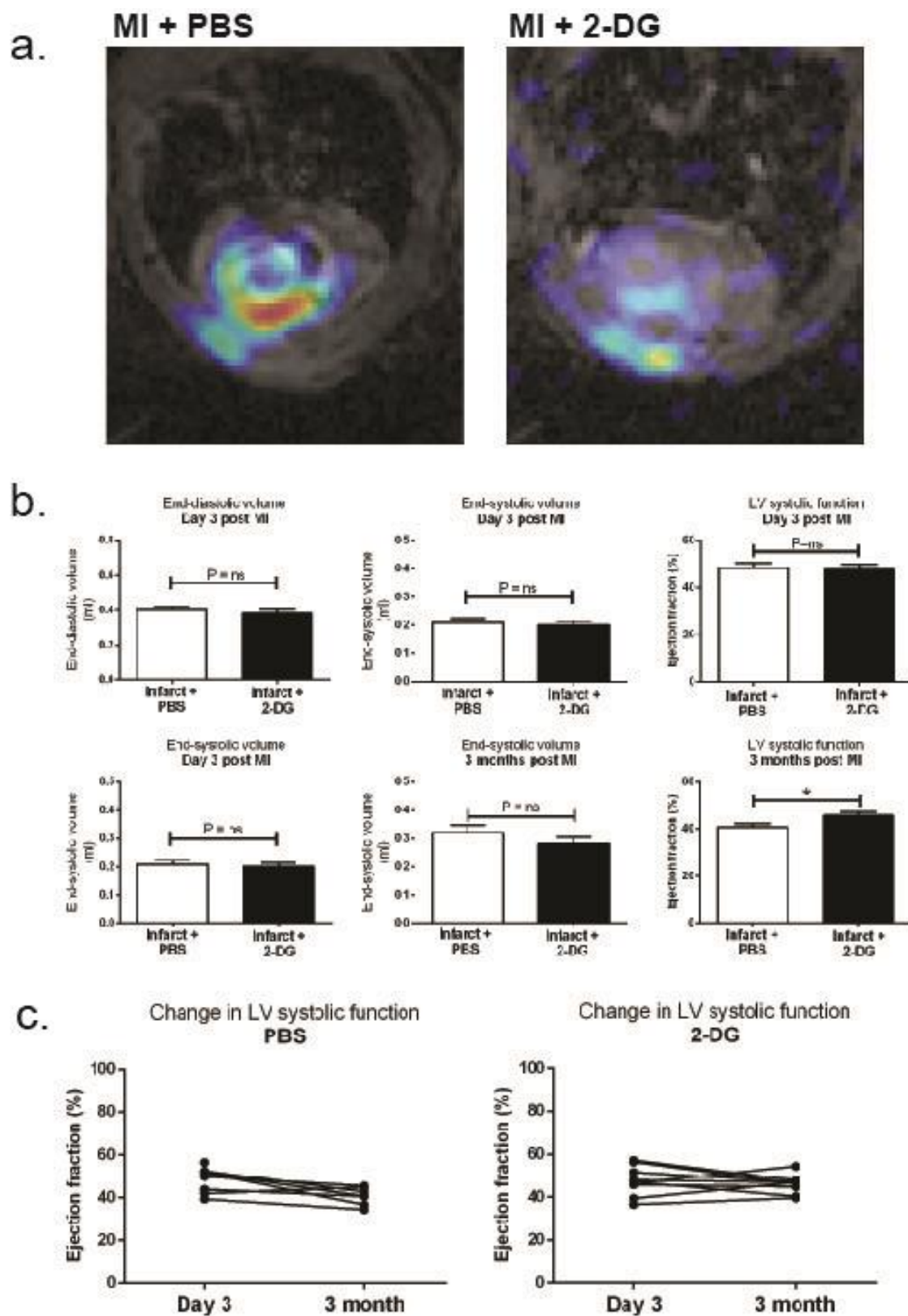
Online Figure II: Cine MRI analysis of left ventricular volumes and function in macrophage depletion experiment.

Online figure III



Online Figure III: A similar pattern of gene regulation with LPS and 2-DG was seen in primary spleen derived macrophages when compared to the RAW264.7 cell line.

Online figure IV



References

1. Atherton HJ, Schroeder MA, Dodd MS, Heather LC, Carter EE, Cochlin LE, Nagel S, Sibson NR, Radda GK and Clarke K. Validation of the in vivo assessment of pyruvate dehydrogenase activity using hyperpolarised ^{13}C MRS. *NMR in biomedicine*. 2011;24:201-208.
2. McKenzie CA, Yeh EN, Ohliger MA, Price MD and Sodickson DK. Self-calibrating parallel imaging with automatic coil sensitivity extraction. *Magnetic Resonance in Medicine*. 2002;47:529-538.
3. Miller JJ, Lau AZ and Tyler DJ. Susceptibility-induced distortion correction in hyperpolarized echo planar imaging. *Magnetic Resonance in Medicine*. 2017.
4. Gudbjartsson H and Patz S. The Rician distribution of noisy MRI data. *Magnetic resonance in medicine*. 1995;34:910-914.
5. Barnett-Vanes A, Sharrock A, Birrell MA and Rankin S. A single 9-colour flow cytometric method to characterise major leukocyte populations in the rat: validation in a model of LPS-induced pulmonary inflammation. *PLoS ONE*. 2016;11:e0142520.
6. Ghugre NR, Ramanan V, Pop M, Yang Y, Barry J, Qiang B, Connelly KA, Dick AJ and Wright GA. Quantitative tracking of edema, hemorrhage, and microvascular obstruction in subacute myocardial infarction in a porcine model by MRI. *Magnetic Resonance in Medicine*. 2011;66:1129-1141.
7. Ghugre NR, Ramanan V, Pop M, Yang Y, Barry J, Qiang B, Connelly KA, Dick AJ and Wright GA. Myocardial BOLD imaging at 3 T using quantitative T2: application in a myocardial infarct model. *Magnetic resonance in medicine*. 2011;66:1739-1747.
8. Lau AZ, Chen AP, Ghugre NR, Ramanan V, Lam WW, Connelly KA, Wright GA and Cunningham CH. Rapid multislice imaging of hyperpolarized ^{13}C pyruvate and bicarbonate in the heart. *Magnetic resonance in medicine*. 2010;64:1323-1331.
9. Lau AZ, Chen AP, Barry J, Graham JJ, Dominguez-Viqueira W, Ghugre NR, Wright GA and Cunningham CH. Reproducibility study for free-breathing measurements of pyruvate metabolism using hyperpolarized ^{13}C in the heart. *Magnetic resonance in medicine*. 2013;69:1063-1071.
10. Zierhut ML, Yen Y-F, Chen AP, Bok R, Albers MJ, Zhang V, Tropp J, Park I, Vigneron DB and Kurhanewicz J. Kinetic modeling of hyperpolarized ^{13}C 1-pyruvate metabolism in normal rats and TRAMP mice. *Journal of magnetic resonance*. 2010;202:85-92.

* Long In Vivo Checklist

*Circulation Research - Preclinical Animal Testing: A detailed checklist has been developed as a prerequisite for every publication involving preclinical studies in animal models. **Checklist items must be clearly presented in the manuscript, and if an item is not adhered to, an explanation should be provided.** If this information (checklist items and/or explanations) cannot be included in the main manuscript because of space limitations, please include it in an online supplement. If the manuscript is accepted, this checklist will be published as an online supplement. See the explanatory [editorial](#) for further information.*

This study involves use of animal models:

Yes

Study Design

The experimental group(s) have been clearly defined in the article, including number of animals in each experimental arm of the study.	Yes
--	-----

An overall study timeline is provided.	No
--	----

The protocol was prospectively written	Yes
--	-----

The primary and secondary endpoints are specified	No
---	----

For primary endpoints, a description is provided as to how the type I error multiplicity issue was addressed (e.g., correction for multiple comparisons was or was not used and why). (Note: correction for multiple comparisons is not necessary if the study was exploratory or hypothesis-generating in nature).	Yes
---	-----

A description of the control group is provided including whether it matched the treated groups.	Yes
---	-----

Inclusion and Exclusion criteria

Inclusion and exclusion criteria for enrollment into the study were defined and are reported in the manuscript.	Yes
---	-----

These criteria were set <i>a priori</i> (before commencing the study).	Yes
--	-----

Randomization

Animals were randomly assigned to the experimental groups. If random assignment was not used, adequate explanation has been provided.	Yes
---	-----

Type and methods of randomization have been described.	N/A
--	-----

Allocation concealment was used.	Yes
----------------------------------	-----

Methods used for allocation concealment have been reported.	Yes
---	-----

Blinding

Blinding procedures with regard to masking of group/treatment assignment from the experimenter were used and are described. The rationale for nonblinding of the experimenter has been provided, if such was not performed.	Yes
---	-----

Blinding procedures with regard to masking of group assignment during outcome assessment were used and are described.	Yes
---	-----

If blinding was not performed, the rationale for nonblinding of the person(s) analyzing outcome has been provided.	Yes
--	-----

Sample size and power calculations

Formal sample size and power calculations were conducted before commencing the study based on <i>a priori</i> determined outcome(s) and treatment effect(s), and the data are reported.	No
---	----

If formal sample size and power calculation was not conducted, a rationale has been provided.	Yes
---	-----

Data Reporting

Baseline characteristics (species, sex, age, strain, chow, bedding, and source) of animals are reported.	Yes
The number of animals in each group that were randomized, tested, and excluded and that died is reported. If the experimentation involves repeated measurements, the number of animals assessed at each time point is provided is provided for all experimental groups.	Yes
Baseline data on assessed outcome(s) for all experimental groups are reported.	Yes
Details on important adverse events and death of animals during the course of the experiment are reported for all experimental groups.	Yes
Numeric data on outcomes are provided in the text or in a tabular format in the main article or as supplementary tables, in addition to the figures.	No
To the extent possible, data are reported as dot plots as opposed to bar graphs, especially for small sample size groups.	Yes
In the online Supplemental Material, methods are described in sufficient detail to enable full replication of the study.	Yes

Statistical methods

The statistical methods used for each data set are described.	Yes
For each statistical test, the effect size with its standard error and <i>P</i> value is presented. Authors are encouraged to provide 95% confidence intervals for important comparisons.	Yes
Central tendency and dispersion of the data are examined, particularly for small data sets.	Yes
Nonparametric tests are used for data that are not normally distributed.	Yes
Two-sided <i>P</i> values are used.	Yes
In studies that are not exploratory or hypothesis-generating in nature, corrections for multiple hypotheses testing and multiple comparisons are performed.	Yes
In "negative" studies or null findings, the probability of a type II error is reported.	N/A

Experimental details, ethics, and funding statements

Details on experimentation including formulation and dosage of therapeutic agent, site and route of administration, use of anesthesia and analgesia, temperature control during experimentation, and postprocedural monitoring are described.	Yes
Both male and female animals have been used. If not, the reason/justification is provided.	Yes
Statements on approval by ethics boards and ethical conduct of studies are provided.	Yes
Statements on funding and conflicts of interests are provided.	Yes

Date completed: 02/04/2018 08:30:22
User pid: 148433